

Investigation of wind-induced dynamic and aeroelastic effects on variable message signs

Debbie Meyer^a, Arindam Gan Chowdhury* and Peter Irwin^b

Department of Civil and Environmental Engineering, Florida International University, Miami, FL, USA

(Received November 9, 2014, Revised April 22, 2015, Accepted April 27, 2015)

Abstract. Tests were conducted at the Florida International University (FIU) Wall of Wind (WOW) to investigate the susceptibility of Variable Message Signs (VMS) to wind induced vibrations due to vortex shedding and galloping instability. Large scale VMS models were tested in turbulence representative of the high frequency end of the spectrum in a simulated suburban atmospheric boundary layer. Data was measured for the 0° and 45° horizontal wind approach directions and vertical attack angles ranging from -4.5° to +4.5°. Analysis of the power spectrum of the fluctuating lift indicated that vertical vortex oscillations could be significant for VMS with a large depth ratio attached to a structure with a low natural frequency. Analysis of the galloping test data indicated that VMS with large depth ratios, greater than about 0.5, and low natural frequency could also be subject to galloping instability.

Keywords: aerodynamic drag; galloping; variable message sign; vortex shedding

1. Introduction

The increasing advancements in Intelligent Transportation Systems (ITS) and the need for more efficient transportation have led to the expanding use of Variable Message Signs (VMS) technology. ITS improve safety and mobility by integrating advanced communication technology into the transportation infrastructure. Variable message signs are a cornerstone of intelligent transportation systems and provide a high tech complement to static flat panel signs. These remotely programmable traffic control devices relay to motorists real-time advisories about changing highway conditions and hazards such as inclement weather, traffic accidents, construction activity, congestion, and public service alerts. Variable message signs are substantially heavier than flat panel aluminum signs and have a larger depth (dimension parallel to the direction of traffic, see Fig. 1). Numerous research studies have investigated wind loading on prismatic rectangular shapes (Bearman and Truman 1972, Laneville *et al.* 1975, Larose and D'Auteuil 2008). However, targeted experimental research to investigate the complex aerodynamic and aeroelastic forces on elevated signs and VMS is very limited. Recent field and wind tunnel studies conducted by Smith *et al.* (2014) and Zuo *et al.* (2014) investigated wind

*Corresponding author, Associate Professor, E-mail: chowdhur@fiu.edu

^aGraduate Student

^bWall of Wind Professor of Practice

induced forces and torques on VMS. Their results indicated that the geometrical configuration of the sign can significantly influence wind loading but their research did not include a dynamic analysis.

The primary load on VMS structures is generally due to wind-induced drag. However, aeroelastic phenomena, caused by the interaction between the wind flow and the structure's vibrational characteristics, can lead to significant vertical forces. These forces may be due to the phenomena of vortex shedding and galloping instability. The resulting vibrations can lead to fatigue damage and ultimately failure of the structure (Kaczinski *et al.* 1998). Note that vortex shedding and galloping responses are characterized by aeroelastic feedback whereby motions of the structure normal to the direction of wind flow affect the flow itself and can amplify the aerodynamic force fluctuations. Analytical and experimental research conducted by Kaczinski *et al.* (1998) and Dexter and Ricker (2002) investigated fatigue loading including vortex shedding and galloping of cantilever VMS support structures. Their results formed the framework for American Association of State Highway and Transportation Officials (AASHTO) fatigue design provisions. Fouad *et al.* (2003 and 2011) extended the research to include fatigue loading and design for non-cantilever VMS supports structures.

VMS structures are relatively new additions to transportation infrastructure and until recently they have not been the subject of rigorous research. Thus the current literature and design specifications do not adequately address the complex aerodynamic and aeroelastic forces on VMS structures. Fouad *et al.* (2003) pointed out that the current Supports Specification (AASHTO) does not adequately address VMS or its supporting structure. With the increasing use of VMS, it is imperative that future versions of the Supports Specifications include adequate guidance and provisions for the design of VMS supporting structures and their foundations. However, very little additional guidance has been added to the current design codes. In addition, the current AASHTO Specification (2013) does not require overhead cantilever or noncantilever structures to be designed for vortex shedding (except during construction and prior to placement of the signs) and only requires cantilever structures to be designed for galloping. The current study focuses on experimental testing conducted at Florida International University's (FIU) Wall of Wind (WOW) facility and data analyses to investigate the susceptibility of VMS to vortex shedding and galloping instability.



Fig. 1 VMS on Florida's Turnpike (photo by D. Meyer)

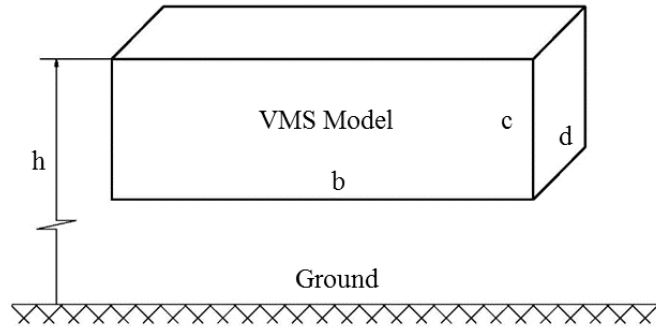


Fig. 2 VMS primary dimensions

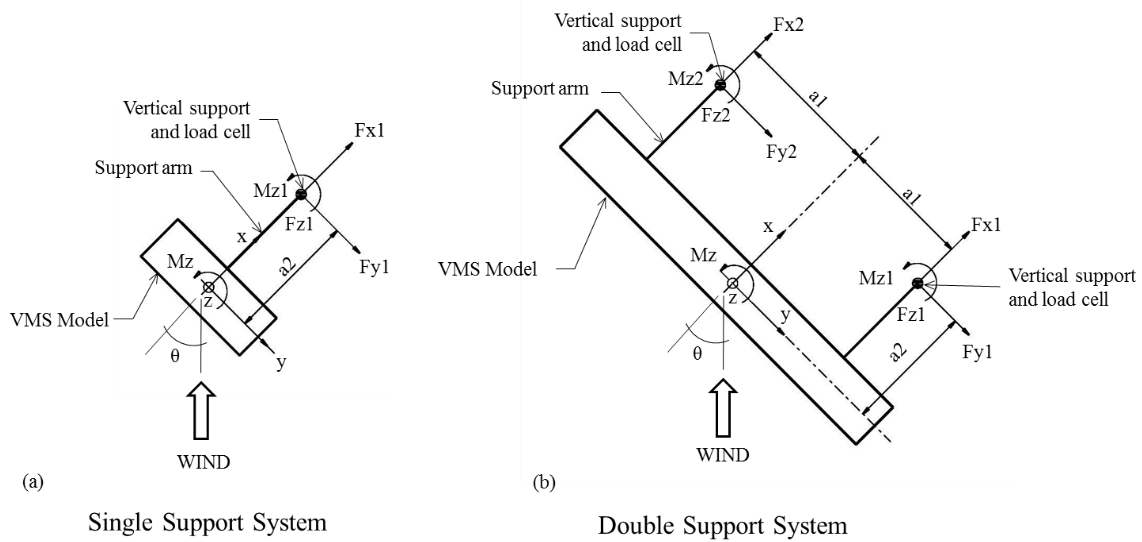


Fig. 3 Force orientation (a) single support configuration (b) double support configuration

1.1 Terminology

Fig. 2 is a schematic representation of an elevated VMS illustrating the model’s primary dimensions: lateral length b , height c , depth (parallel to highway dimension) d , and the distance from the ground to the top of the model h . Geometric ratios used throughout this study were

$$\text{Aspect ratio} = b/c \tag{1}$$

$$\text{Depth ratio} = d/c \tag{2}$$

$$\text{Clearance ratio} = c/h \tag{3}$$

Two model support configurations were used for testing. The models were mounted on cantilever support masts which incorporated load cells. Two support masts were used for the longer models and a single support mast was used for the shorter models. Fig. 3 shows the axes and force orientation for the single and double support configuration used throughout the study.

Body-axes have been used in this study as shown. The x-axis is positive in the highway direction and the y-axis is positive to the right. The z-axis is positive in the upward direction and counterclockwise is positive for the twisting moment M_z . The forces and moments measured by individual load cells for this study are also shown. Angle θ defines the horizontal wind approach direction and 0° is defined as wind normal to the front face of the model.

1.2 Background

1.2.1 Vortex shedding

Vortex shedding occurs during steady uniform flow when alternating vortices are periodically shed into the wake of a structure. The alternating pattern of vortices is commonly referred to as von Kármán vortex street. The frequency at which the vortices are shed (f_s) is proportional to the approaching mean wind speed (\bar{U}) and inversely proportional to the height (c) of the structure. This is expressed non-dimensionally as the Strouhal number

$$S_t = \frac{f_s c}{\bar{U}} \quad (4)$$

The Strouhal number for a circular cross section depends on the Reynolds number of the oncoming flow but for sharp edged cross sections like VMS, where flow separation occurs at the leading edge, the Reynolds number effects are not expected to be significant. However, the Strouhal number for sharp edged rectangular cross sections has been shown to be a function of the depth ratio (Taylor *et al.* 2014, Cao *et al.* 2014, Liu and Kopp 2010). A relationship between the Strouhal number and depth ratio for rectangular cross sections was developed by Dyrbye and Hansen (1997). Since VMS are principally rectangular prismatic shapes, their Strouhal number should be in the range of 0.06 to 0.15 (Ginal 2003).

Parkinson (1989) compiled results from Brooks (1960), Hoerner (1965), Nakamura and Tomonari (1977), and Washizu *et al.* (1978) and showed how the Strouhal number is affected by the depth ratio. For smooth flow and a depth ratio in the range of $0 < d/c < 1.0$, the base pressure changes abruptly with increasing d while the Strouhal number only changes slightly. An explanation for this is provided by Bearman and Trueman (1972). If d is small enough, the downstream edges of the afterbody will not interfere with the inward curvature of the streamlines and full strength vortices will form closer to the rear of the cylinder. This lack of interference with the shear layers is why the Strouhal number is not significantly affected. When d is sufficiently large, the downstream edges of the after body will begin to interfere with the inward curvature of the streamlines forcing the vortices to form further downstream and the shear layers to be more diffused. This results in a smaller vortex shedding frequency and a drop in the Strouhal number (Gerrard 1966). Reattachment of flow along the sides of the after body results in an increase in base pressure and a sharp increase in the Strouhal number. The abrupt change arises due to the decrease in lateral spacing of the shear layers after separating from the downstream corners. Smaller lateral spacing of the shear layers corresponds to a smaller stream wise spacing of vortices and therefore a larger vortex shedding frequency (Parkinson 1989).

The alternating shedding of vortices produce periodic forces that result in oscillations in a plane

normal to the direction of wind flow. Significant oscillation can occur when the frequency of vortex shedding is close to the natural frequency of a flexible structure. These lateral vibrations have a strong organizing effect on the vortex shedding pattern which can increase the strength of the vortices and couple the vortex shedding frequency to the natural frequency of the structure. This phenomenon is known as lock-in. The critical wind speed (U_{cr}) at which lock-in occurs can be estimated using the Strouhal number relation

$$U_{cr} = \frac{f_n c}{S_t} \tag{5}$$

where in this case f_n is the natural frequency of the structure. The amplitude of the vibrations resulting from lock-in is limited by the balance between the energy input into the motion by the vortices and the dissipation of that energy by structural damping. Eventually large oscillations of the structure interfere with the uniform shedding of vortices and therefore the maximum amplitude of vortex induced vibrations may be self-limiting (Blevins 1977). The drag force on a structure vibrating at or near the vortex shedding frequency is also a function of vibration amplitude. Bearman and Obasaju (1982) showed that drag on a square structure increases at resonance.

The range of wind speeds at which vortex shedding can occur is bounded by the ability of the vortices to stay locked onto the structural motion. According to the commentary in the AASHTO Specification (2009), vortices shed at wind velocities below approximately 5 m/s do not possess sufficient energy to excite most sign support structures and at wind speeds greater than about 20 m/s the natural turbulence in the flow disturbs the formation of vortices. This would imply VMS structures are susceptible to vortex induced vibrations only for the range of wind speeds between 5 m/s and 20 m/s. In fact there is little evidence that the turbulence intensity increases with wind speed. Therefore vortex excitation at speeds above 20 m/s cannot be discounted.

1.2.2 Galloping

Galloping of a prismatic structure is the self-excited response to natural wind due to the aeroelastic instability of the structure. Galloping is typically characterized by predominately horizontal wind flow and vertical motion of the structure. To initiate galloping there must be an initial displacement of the structure that changes the angle of attack (α) of the wind flow relative to the structure. The initial displacement may be due to fluctuations in the wind or vortex shedding. The vertical velocity (\dot{z}) of the structure results in the angle of attack of the wind being

$$\alpha = \arctan\left(\frac{\dot{z}}{\bar{U}}\right) \tag{6}$$

where \bar{U} is the horizontal velocity of the oncoming wind. For $\dot{z} \ll \bar{U}$ this becomes

$$\alpha = -\left(\frac{\dot{z}}{\bar{U}}\right) \tag{7}$$

Let C_L denote the lift coefficient, α the angle of attack, and C_D the drag coefficient. The equations of motion of the body yield the *necessary* condition for incipient galloping motion, known as the Den Hartog criterion

$$\left[\frac{dC_L}{d\alpha} + C_D\right]_{\alpha=0} < 0 \tag{8}$$

where the left-hand side of Eq. (8) is evaluated at $\alpha = 0$. A small vertical motion of the structure results in a force given by

$$F_z = -\frac{1}{2}\rho\bar{U}\dot{z}A\left(\frac{dC_L}{d\alpha} + C_D\right)_{\alpha=0} \quad (9)$$

The force is in the same direction as the body velocity \dot{z} if $dC_L/d\alpha + C_D < 0$ and is proportional to that velocity. Therefore it is effectively a negative aerodynamic damping force. The sufficient condition for incipient galloping motion is that this force exceed the positive damping force due to the mechanical damping. It follows from this condition that the minimum wind speed required to initiate galloping is proportional to the mechanical damping of the structure (Novak 1972).

Parkinson (1963) explained that flow reattachment will occur along side of a prismatic shape for sufficiently large values of α . The galloping characteristics of the structure will be affected by the resulting asymmetry in the pressure distribution which produces a net force in the vertical direction. Parkinson (1989), using data from Brooks (1960), Smith (1962), Laneville (1973), Novak (1974), and Nakamura and Tomonari (1977), showed that rectangular cylinders with $d/c < 0.75$ in smooth flow did not gallop from rest (hard galloping) and required an initial vibration. Sections in the range $0.75 < d/c < 3.0$ did gallop spontaneously from rest (soft galloping). The lower boundary for the beginning of soft galloping corresponds to the abrupt change in base pressure noted previously when the trailing edges of the afterbody begin to interfere with the inward curvature of the streamlines. For $d/c > 3.0$ no galloping could be induced. This upper boundary corresponds to an afterbody length that is sufficiently long for reattachment of the shear layer to occur. Parkinson (1989) also demonstrated that as turbulence in the oncoming flow is increased, soft galloping sections experience weaker galloping and eventually become stable and hard galloping sections become soft galloping.

Kaczinski *et al.* (1998) had difficulty reproducing galloping results in wind tunnel experiments. A model observed to gallop in one test did not gallop in another test under identical test conditions. The same unpredictability has been observed in the field. Only one structure experienced galloping in a series of structures subjected to the same wind conditions. The researchers attributed the difficulty in reproducing galloping results in the laboratory and the unpredictability observed in the field to the sensitivity of these structures to very specific conditions such as the dynamic properties of the structure, aerodynamic properties of the attachments, and flow characteristics (Kaczinski *et al.* 1998). In-service VMS attached to cantilever support structures with fundamental frequency of 1.04 – 1.10 Hz and mechanical damping ratio of 0.4 – 0.7% have been observed galloping, indicating that the flow velocity was high enough to induce the aerodynamic damping ratio required for galloping to occur. Structural failure due to galloping was documented for a bent monopole structure in California in 1995. Instrumentation and monitoring of this structure showed that it was galloping in steady winds (Dexter and Ricker 2002). The susceptibility of non-cantilever (i.e., bridge-type) VMS support structures to galloping is still unclear. Dexter and Ricker (2002) did not expect VMS mounted on non-cantilever structures to be susceptible to galloping “due to the rigidity of the sign bridge.” Fouad *et al.* (2003) points out that the question of susceptibility of non-cantilever support structures to galloping (and vortex shedding) is unresolved and additional laboratory testing and field evaluation is necessary. However, Fouad *et al.* (2003) did not specifically address VMS.

Ginal (2003) evaluated the galloping instability of two non-cantilever four chord VMS support structures in Wisconsin. Each structure supported a VMS with dimensions corresponding to geometric ratios of $b/c \approx 3$ and $d/c \approx 0.5$. A modal analysis using FEM was performed and the onset wind velocities were determined using the universal galloping response curves for rectangular prisms developed by Novak and Tanaka (1974). Based on calculations and assumptions by Ginal (2003), the onset wind velocities for the two structures were greater than 98

m/s. Given these high velocities, Ginal (2003) concluded that galloping vibrations do not need to be considered as a loading scenario for the non-cantilevered VMS support structure as configured in his test group. He adds, however, that since galloping of sign support structures is highly dependent on the characteristics of the structure including cross section, total damping ratio, and natural frequencies as well as flow characteristics, a wind tunnel study should be conducted to validate the results of his research.

2. Description of the experimental set up and testing procedure

2.1 Wall of wind facility

The experiments were conducted in the WOW facility at FIU. The test section of this open jet system is 6.1 wide x 4.3 m high and wind is generated by two rows of six electric fans arranged in a convex arc. The wind flow from the fans merges into a contraction zone which is designed to generate a high velocity uniform flow field. Vertical vanes at the contraction exit guide the flow in the longitudinal direction. A 9.8 m flow simulation box consisting of triangular spires and floor roughness elements help develop the desired atmospheric boundary layer (ABL) profile.

Tests were conducted on 1:3 scale models in a simulated suburban atmospheric boundary layer at mean wind speeds of 15 m/s and 40 m/s. The turbulence intensity at the model mounting height of 2.3 m was approximately $I_u \approx 8\%$. The turbulence intensity of the WOW laboratory flow is lower than the full-scale target suburban terrain ABL. This is due to the partial turbulence simulation method that is utilized in the WOW which reproduces only the high frequency portion of the ABL spectrum (see Yeo and Gan Chowdhury 2013, Fu 2013). The partial turbulence simulation utilized in the WOW is governed by the following formula provided by Irwin (1998)

$$\frac{I_{um}}{I_{up}} = \left(\frac{L_{um}}{L_{up}} \right)^{\frac{1}{3}} \left(\frac{b_p}{b_m} \right)^{\frac{1}{3}} \quad (10)$$

where I_u is the turbulence intensity, L_u is the integral length scale and b is the reference length. The subscripts m and p denote model and prototype, respectively. More information about the partial turbulence simulation method used in the WOW and the validation of aerodynamic results can be found in Irwin (1998), Fu *et al.* (2012), Yeo and Gan Chowdhury (2013), and Fu (2013). The low-frequency portion of the spectrum, which is absent from the flow used in these tests, would have the effect of slightly amplifying the vortex-induced and galloping oscillations. To the extent that the results of this investigation would warrant the conclusion that VMS vortex-induced and/or galloping oscillations are possible under certain conditions, this conclusion would be reinforced if low-frequency flow fluctuations were taken into account.

2.2 Experimental design

2.2.1 Model and support configuration

Tests were conducted in the WOW to determine mean longitudinal, lateral, and vertical lift coefficients that were used to investigate the susceptibility of VMS to vortex shedding and galloping. A total of 13 models were constructed for drag coefficient testing but only three models were used to investigate aerodynamic instability. The model dimensions were 0.6 x 0.6 x 0.4 m, 1.8 x 0.6 x 0.4 m, and 3.0 x 0.6 x 0.4 m which corresponded to geometric ratios of $b/c = 1, 3,$ and 5

and $d/c = 0.7$. The models were constructed from 13mm shop grade maple plywood and supported with a steel single or double cantilever system which was rigidly bolted to the WOW facility floor. A series of wedges were used to attach the model to the support system 2.3 m above the WOW facility floor ($c/h = 0.24$). The wedges were positioned to simulate vertical wind approach angles of $\alpha = -4.5, -2.5, 0, 2.5, \text{ and } 4.5$. Additional stability was provided by three wire cables attached to eye bolts at the top of each vertical support (below the load cells) and fixed to the WOW floor.

The primary focus of this study was investigation of wind-induced dynamic, aeroelastic effects on VMS. Consequently, only the VMS, and not the truss structure (see Fig. 1), was modeled for testing. It is recognized that the mutual interaction of the sign and the truss structure was not taken into account. However, it is to be noted that the standard design procedure uses separate aerodynamic coefficients for the sign and the support structure, thus it also neglects the interaction effect.

2.2.2 Instrumentation

A multi-axis load cell supplied by JR3, Inc. (model 75E20S4 – M125D – AF 1350L) was mounted on top of the vertical support to simultaneously measure forces, moments and torques. The load cells are equipped with six degree of freedom force and torque sensors which simultaneously measure forces along three orthogonal axes ($x, y, \text{ and } z$) and moments and torques about those axes.

Cobra probes supplied by Turbulent Flow Instruments were used to measure the wind velocity and turbulence in three orthogonal directions. Probes were mounted vertically 0.9 m above the model at an elevation of 3.5 m above the WOW floor.

2.3 Tare tests

Tare tests were conducted to isolate and correct for secondary aerodynamic forces applied to the support system. Tare test data was sampled at 100 Hz for 1 minute and were tested for horizontal wind approach directions of 0° and 45° . Baseline data sampled one minute before and one minute after each test run was subtracted from the measured test data.

2.4 Wind field adjustments

2.4.1 Wind speed spatial relationship

The mean wind speed (\bar{U}) used in the calculation of the drag coefficient was determined by averaging the mean temporal wind speed measured at different locations during model testing. This was done as follows. Wind speed measurements were recorded during each test run using three cobra probes mounted at the reference height of 3.5 m, which is 0.9 m above the model. The probes were spaced horizontally 1.2 m apart with the middle probe centered with respect to the model. The mean temporal wind speed for the one minute test length was determined for each probe. Analysis of the mean temporal wind speeds for each probe showed that the wind profile along the horizontal length of the model was not quite uniform. The measured wind speed at the center probe was approximately 4% higher than the wind speeds measured at each of the two outer probes for the 0° horizontal wind direction and 5% higher for the 45° wind direction. Consequently, a linear interpolation was applied to calculate the wind speed at the horizontal location corresponding to the outer edge of each model. These three spatial wind speeds (left edge, center, and right edge) were averaged to determine the mean spatial wind speed at the reference height of 3.5 m. This is the wind speed used in the force coefficient calculation.

2.4.2 Free flow wind

Free flow wind speed measurements were conducted to determine the relationship between the wind speeds at the reference height of 3.5 m and the desired wind speeds at the model mounting height of 2.3 m. The free flow wind testing used an array of cobra probes mounted on a grid of vertical and horizontal uni-strut supports. The ratio of the measured free flow wind speed at 3.5 m to the mean wind speed at 2.3 m was established for each set of corresponding cobra probes. The drag coefficient calculation was adjusted to the mounting height wind speed by multiplying the calculated drag coefficient at 3.5 m by the mean wind speed ratio squared.

2.4.3 Blockage

A blockage test was performed to obtain an overall measure of whether the wind speed measurements were sampled sufficiently far enough away and to correct for local flow effects. The blockage test consisted of testing a model with dimensions of 3.0 x 0.6 m at a wind speed of 19 m/s and another model which was 1/4 blockage (1.5 x 0.3 m), at twice the wind speed (38 m/s). Both models were flat panels ($d = 13$ mm) with $b/c = 5$. The measured wind speed at the reference height of 3.5 m was intended to be far enough away from the models to avoid the local flows. However, the tests revealed that the measurements may not have been completely free of local effects. Tests using the larger model (1:3 scale) showed that it was probably still in a slightly accelerated local flow. This caused the drag coefficient results to be slightly low. For the smaller model at half the scale (1:6), the flows were less affected which resulted in larger drag coefficients. From the data for the two blockage ratios the drag coefficient for zero blockage was obtained by extrapolation. Using the assumption that the blockage correction was proportional to the area ratio (A/A_s), where A = frontal area of test specimen and A_s = area of test section cross-section, the blockage corrections for all other test specimens were evaluated and applied.

2.5 Testing procedures

Force coefficient tests were conducted at wind speeds of 15 m/s and 40 m/s in the simulated suburban boundary layer for the 0° and 45° horizontal wind approach directions. Zero degree was defined as the direction of the approaching wind normal to the front face of the model. The ambient temperature and air pressure readings were monitored and updated before each test. Data was sampled at 100 Hz for 1 minute for each test run. Baseline data sampled one minute before and one minute after each test run was subtracted from the measured test data. The appropriate tare correction, blockage correction, and wind speed adjustments were applied to all test data. The complete results for the drag coefficient testing are discussed in a separate report.

Time history data was used to compute the power spectra of the fluctuating lift for models with $d/c = 0.7$. Galloping tests were conducted using the model with dimensions 3.0 x 0.6 x 0.4 m ($b/c = 5$, $d/c = 0.7$) for the 0° horizontal wind direction and vertical wind attack angles of $\alpha = -4.5, -2.5, 0, 2.5,$ and 4.5 . The model was tested at wind speeds of 15 and 40 m/s. The test conditions and procedures were identical to those used for all other force coefficient tests. Fig. 4 shows a picture of the galloping test setup in the WOW.

3. Predictions of vortex shedding amplitudes from spectra of lift

Vortices shed from the upper and lower edges of the VMS cause fluctuating forces primarily in

the crosswind direction. The simplest theory for predicting vortex excitation assumes the excitation force oscillates in time t in a pure sinusoidal manner, with the excitation force per unit length being given by

$$f(t) = \frac{1}{2}\rho U^2 c C_L' \sin \omega_v t \quad (11)$$

in which C_L' is a fluctuating “lift coefficient”, c = cross-section width normal to wind, and

$$\omega_v = 2\pi N_v \quad (12)$$

where N_v is the shedding frequency of the vortices. Note that Eq. (11) ignores feedback effects that cause the vortices to be locked on to the structure’s motions. Since the present tests were on a rigid model the feedback effects could not be evaluated. Therefore the present estimates of vortex shedding amplitudes are based on the assumption that feedback effects are small and, if the vortex shedding frequency is equal or close to the frequency of vibration of the structure, could underestimate actual amplitudes.

Considering crosswind motions in the direction, z , the deflection $z(y,t)$ of the structure in each of its natural modes of vibration may be expressed as

$$z(y,t) = \phi(y)q(t) \quad (13)$$

where $\phi(y)$ = deflection shape of the mode of vibration, and $q(t)$ = generalized coordinate for the mode of vibration. It can then be shown that the equation of motion in a particular mode of vibration is

$$M_G(\ddot{q} + 2\bar{\omega}_0\zeta\dot{q} + \bar{\omega}_0^2q) = F_G(t) \quad (14)$$



Fig. 4 Test setup in the WOW (Photo by D. Meyer)

where

$$M_G = \text{generalized mass} = \int_0^L m(y)\phi(y)^2 dy \tag{15}$$

and

$$F_G = \text{generalized aerodynamic force} = \int_0^L f(y,t)\phi(y)dy \tag{16}$$

where m = mass per unit length, and L = length of structure. For simplicity, it is assumed that the force fluctuation is uniform along the length of the structure and Eq. (16) becomes

$$F_G = \frac{1}{2}\rho U^2 C_L' c \times \int_0^L \phi dy \times \sin(\omega_v t) \tag{17}$$

The solution to Eq. (14) can be obtained by assuming

$$q = q_0 \sin(\omega_v t + \varphi) \tag{18}$$

where φ = phase angle, which leads to a predicted maximum response when $\omega_v = \omega_o$, with the amplitude being

$$|q_0| = \frac{\frac{1}{2}\rho U^2 C_L' c \int_0^L \phi dy}{\omega_v^2 M_G 2\zeta} \tag{19}$$

If the mass distribution is uniform then this becomes

$$|q_0| = \frac{\rho U^2 C_L' c \int_0^L \phi dy}{4\omega_v^2 m\zeta} \times \frac{\int_0^L \phi dy}{\int_0^L \phi^2 dy} \tag{20a}$$

Eq. 20(a) implies that if the mode shape ϕ were anti-symmetric, as for a complete sine wave for example, then the response would be zero. In fact, the rotation of the vortices often is able to switch sign when the mode shape changes sign and a response still occurs (Farquharson *et al.* 1950). Therefore, recognizing this, ϕ is replaced in the numerator of Eq. 20(a) by its absolute value. Also, variables can be grouped into non-dimensional parameters that help in assessing when vortex excitation might be a problem.

$$\frac{|q_0|}{c} = \frac{C_L'}{16\pi^2} \left(\frac{U}{N_v c}\right)^2 \left(\frac{\rho c^2}{m\zeta}\right) \times \frac{\int_0^L |\phi| dy}{\int_0^L \phi^2 dy} \tag{20b}$$

The parameter $4\pi m\zeta/\rho c^2$ has been named the Scruton number (S_c) after Scruton, who first identified it as a key parameter by which to assess the susceptibility of a structure to vortex excitation. It has also often been expressed as $2m\delta/\rho c^2$ where δ = the logarithmic decrement, which equals $2\pi\zeta$ for the low values of ζ of interest in wind engineering. The higher the Scruton number the less will be the amplitude of the vortex-excited motion.

Also, from Eq. 20(b), the parameter $N_v c/U$ is the Strouhal number, S_s . Therefore Eq. 20(b) can be expressed as

$$\frac{|q_0|}{c} = \frac{C_L'}{4\pi S_s^2 S_c} \times \frac{\int_0^L |\phi| dy}{\int_0^L \phi^2 dy} \tag{20c}$$

From the power spectra of the fluctuating lift obtained on VMS with $d/c = 0.7$ a peak in the excitation spectrum was noted at a non-dimensional frequency $f_c/U = 0.10$. This may be identified

as the Strouhal number for the VMS. From the spectra included in Figs. 5(a)-5(c), the area under the peak was measured and the lift coefficients determined (refer to Table 1).

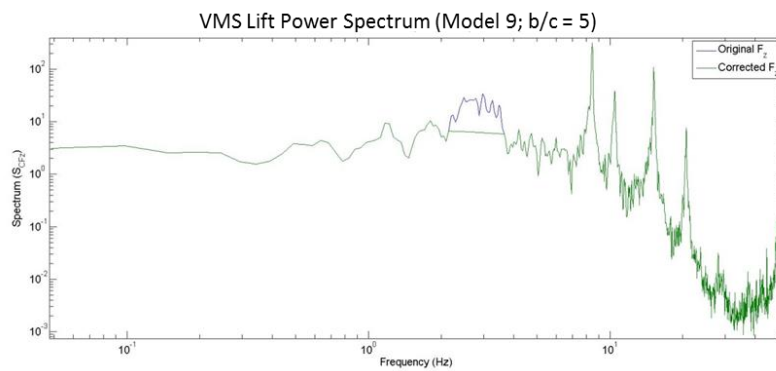


Fig. 5(a) VMS lift power spectrum for Model 9 with $d/c = 0.7$

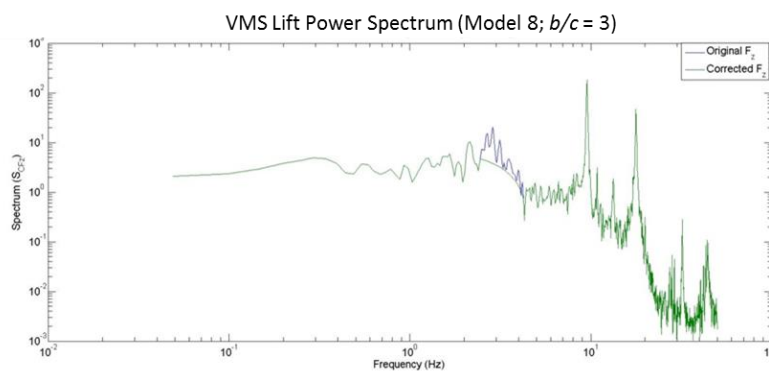


Fig. 5(b) VMS lift power spectrum for Model 8 with $d/c = 0.7$

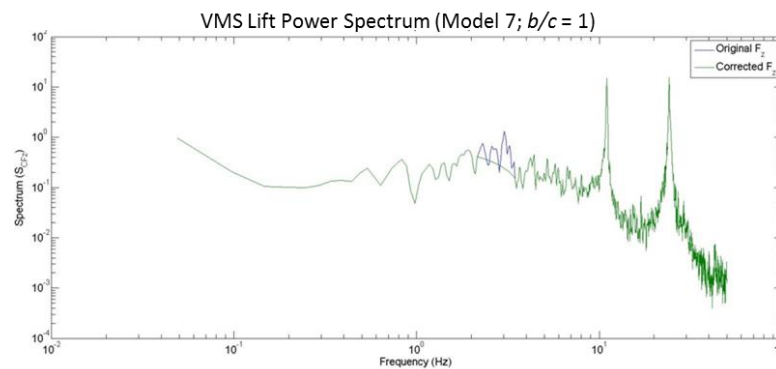


Fig. 5(c) VMS lift power spectrum for Model 7 with $d/c = 0.7$

Table 1 Strouhal Number, Scruton Number, and vertical lift coefficient

b/c	S_t	S_c	C'_L
1	0.10	4.9	0.035
3	0.10	4.9	0.046
5	0.10	4.9	0.052

In estimating the Scruton Number S_c , the damping ratio was taken as 0.005, the vertical dimension as 1.8 m and the weight per unit length of the VMS as 201 kg/m. The weight of the truss was assumed to be approximately 217 kg/m. As suggested by Ginal (2003), the entire mass of the VMS and 50% of the mass of the truss was used in the calculation. With knowledge of the natural frequency and the inputs from Table 1, the amplitude of oscillation of the VMS due to vortex excitation can be estimated using Eq. (19(c)). The ratio of integrals in Eq. (20(c)) was taken to be that for a sinusoid, i.e., $4/\pi \approx 1.27$

Based on the above calculations, a sign with $c = 1.8$ m and $b = 9.1$ m is predicted to experience vertical sinusoidal oscillations due to vortex shedding with an amplitude of about 203 mm. The predicted 3 second gust speeds where oscillations would start to build to the 203 mm amplitude are plotted as a function of the natural frequency in Fig. 6. Vortex oscillations take some time to build up and the gust speeds plotted here are used only as an indicator of when the accompanying sustained speeds are sufficient to generate oscillations.

These results were obtained for $d/c = 0.7$, which is expected to be the worst case since it has the largest horizontal area for the vortices to act on. While lift spectra were not obtained for the other d/c values, the vertical excitation forces are expected to be reduced roughly in proportion to the plan area of the sign, i.e., for $d/c = 0.4$ an amplitude of approximately 116 mm would be expected. At $d/c=0.1$ the amplitude is expected to reduce further but the plan area of the support structure would then be comparable to that of the sign, so a straight proportional reduction is probably no longer valid. From the above discussion it can be concluded that if the natural frequency is low, significant vortex induced oscillations are possible for VMS with 1.8 m vertical dimension within the wind speed ranges of concern.

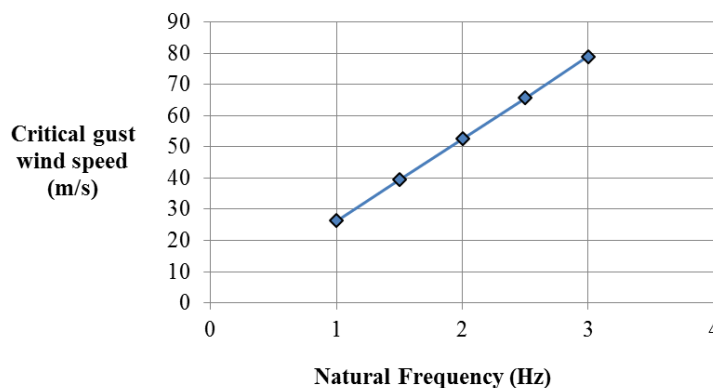


Fig. 6 Critical gust speed in winds that will cause vortex shedding oscillations for $c = 1.8$ m

4. Prediction of the onset wind velocity for galloping

Galloping susceptibility was investigated for a VMS with $d/c = 0.7$. Fig. 7 is a graph showing the variation of C_L (vertical lift coefficient) and C_D (normal force coefficient) as a function of the wind angle of attack (α). The graph shows that the slope of C_L is negative in the range $-4.5^\circ < \alpha < 4.5^\circ$. For the test wind speed of 15 m/s wind speed, the slope of C_L (i.e., $dC_L/d\alpha$) is -2.31 and $C_D = 1.19$ at $\alpha = 0^\circ$.

Evaluation of the Den Hartog criterion yields

$$\frac{dC_z}{d\alpha} = \left[\frac{dC_L}{d\alpha} + C_D \right]_{\alpha=0} < 0 = -1.12 \tag{21}$$

This suggests the VMS, as configured, does have the potential for galloping.

The critical galloping onset wind velocity (U_{crit}) for a typical span truss VMS support structure was calculated. Starting with the vertical force per unit length being given by

$$Z = \frac{1}{2} \rho U^2 c \left[\frac{dC_z}{d\alpha} \right]_{\alpha=0} \alpha \tag{22}$$

and

$$\alpha = -\frac{\dot{q}}{U} \tag{23}$$

Therefore

$$Z = -\frac{1}{2} \rho U^2 c \frac{dC_z}{d\alpha} \frac{\dot{q}}{U} \tag{24}$$

Assuming the vertical mode of vibration for the structure can be modeled as a SDOF oscillator, the equation of motion including the aerodynamic force in the vertical direction can be written

$$M_G(\ddot{q} + 2\omega_0\zeta\dot{q} + \omega_0^2q) = - \int_{sign} \frac{1}{2} \rho U^2 b \frac{dC_z}{d\alpha} \cdot \frac{\dot{q}}{U} \phi^2 dy \tag{25}$$

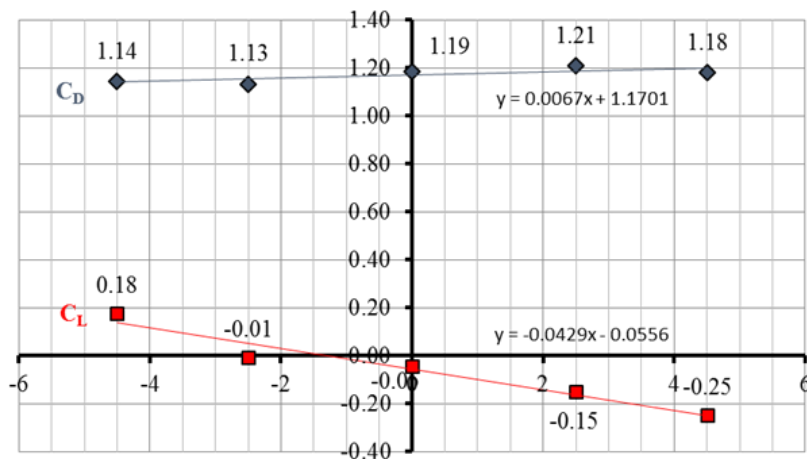


Fig. 7 Graph of C_D and C_L versus vertical approach angle

Rearranging the equation and combining the right hand term with the \dot{q} term on the left yields

$$M_G(\ddot{q} + 2\omega_0\dot{q}\left(\zeta + \frac{\rho U \int_{\text{sign}} b \frac{dC_Z}{d\alpha} \phi^2 dy}{4\omega_0 M_G}\right) + \omega_0^2 q) = 0 \quad (26)$$

The $dC_Z/d\alpha$ term is assumed to be zero along parts of the structure where the VMS is not present. Therefore the integral is only evaluated over the part of the structure where the VMS is present. From Eq. (26), the total damping of the system becomes

$$\zeta_{\text{total}} = \zeta + \frac{\rho U \int_0^b c \frac{dC_Z}{d\alpha} \phi^2 dy}{4\omega_0 M_G} \quad (27)$$

where ζ is the structural damping ratio, ρ the density of air, b is the length of the VMS, c is the height of the VMS, $dC_Z/d\alpha$ is the slope of C_Z at 0, ϕ^2 is the modal deflection shape, ω_0 is the natural circular frequency and M_G is the generalized mass. At critical velocity the total damping of the system is zero

$$\zeta + \frac{\rho U_{\text{crit}} \int_0^b c \frac{dC_Z}{d\alpha} \phi^2 dy}{4\omega_0 M_G} = 0 \quad (28)$$

where U_{crit} is the onset wind velocity for galloping. Solving Eq. (28) for the critical velocity yields

$$U_{\text{crit}} = -\frac{4\zeta\omega_0 M_G}{\rho \int_0^b c \frac{dC_Z}{d\alpha} \phi^2 dy} \quad (29)$$

Since the mass is assumed constant along the length of the VMS, U_{crit} becomes

$$U_{\text{crit}} = -\frac{4\zeta\omega_0 M_G}{\rho b c \frac{dC_Z}{d\alpha} \phi^2} \text{ for } \frac{dC_Z}{d\alpha} < 0 \quad (30)$$

Eq. (30) was used to estimate the critical galloping onset wind velocity for a typical VMS support structure. The structure consisted of a 3-chord steel truss 1.8 m high x 1.5 m deep with a horizontal truss span of 30.5 m. The weight of the truss was increased 5% to account for the additional weight of connections. A 9.1 m long x 1.8 m high x 1.2 m deep walk-in style VMS was assumed for this calculation. The mass of the VMS was assumed to be 201 kg/m and the mass of the truss (including a catwalk and 5% additional for connections) was assumed to be 217 kg/m. The entire mass of the VMS and 50% of the mass of the truss was used in the critical onset wind velocity calculation. Damping ratios (ζ) from 0.0025 to 0.0075 and natural frequencies (f) from 0.8 to 3.0 Hz were used to cover a wide range of conditions.

Using Eq. (30) and the parameters in Table 2 with $dC_Z/d\alpha = -1.12$, the critical galloping onset wind velocity (U_{crit}) was calculated and graphed in Fig. 8. Results ranged from 12 m/s for the most flexible structures to 129 m/s for the least flexible structures. The U_{crit} result of 55 m/s obtained in the present study for a VMS with $f = 2.4$ and $\zeta = 0.4\%$ is lower than the U_{crit} result of 98 m/s determined by Ginal (2003) for a structure with comparable aerodynamic parameters. However, the depth ratio of the VMS in the FIU WOW study was $d/c = 0.7$ and the depth ratio for the Ginal (2003) structure was $d/c = 0.5$. The lower critical wind speed result for the WOW study was anticipated since according to Parkinson (1963) there is an increased potential for shapes with a longer afterbody length to gallop. This occurs because the afterbody length interferes with the vortex formation in the downstream wake region. Flow that separates from the windward edges

can reattach along one side of the afterbody length which leads to an asymmetric surface pressure distribution and a net force in the z -direction. Since the resulting galloping instability is a function of the afterbody length, the results of this study based on $d/c = 0.7$ is expected to be lower than Ginal (2003) which was based on $d/c = 0.5$. Since the galloping onset wind velocity for structures with low natural frequency and low critical damping is in the range of likely wind speeds experienced in many areas of the country, it is suggested that galloping potential be investigated further and considered in the design of VMS structures.

5. Conclusions

- Analysis of the power spectra of the fluctuating lift for a VMS with $d/c = 0.7$ indicated that vertical vortex shedding oscillations could be significant for a VMS with a large depth ratio attached to a structure with a low natural frequency.
- Evaluation of the Den Hartog criteria and determination of the onset wind velocity for galloping, indicated that the model configured with geometric ratios of $b/c = 5$ and $d/c = 0.7$ is susceptible to galloping instability. Based on this finding, galloping is also possible for a VMS with a large depth ratio attached to a flexible structure with a low natural frequency.
- A recent review and experiments conducted by Mannini *et al.* (2014) further supports the above conclusions that elongated shapes such as VMS maybe susceptible to aeroelastic instability. The study indicated that both vortex induced vibration and galloping are possible for elongated prismatic shapes with dimensions similar to VMS with large depth ratios. The study also suggested that a strong interaction between the two phenomena may arise for a range of Kármán vortex resonance and galloping wind speeds that are consistent with the estimated parameters and wind speeds obtained in the FIU WOW. It is therefore suggested that future research is conducted using a dynamic rig to investigate this interaction further.

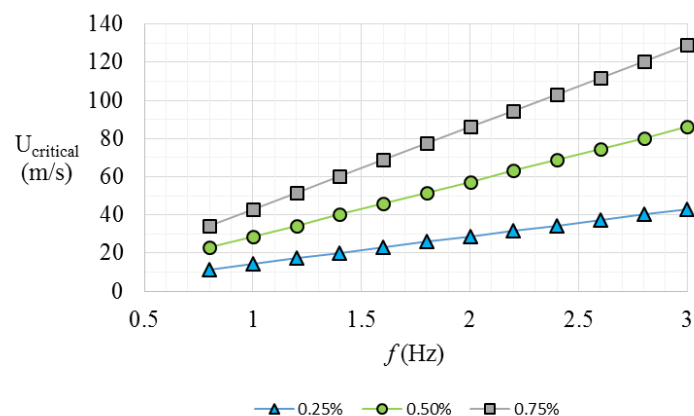


Fig. 8 Critical galloping onset wind velocity as a function of natural frequency

Table 2 Parameters for critical galloping onset wind velocity calculation

ρ (kg/m ³)	c (m)	b (m)	Span (m)	m_{VMS} (kg/m)	M_{truss} (kg/m)	φ	ζ (%)	F (Hz)
1.227	1.8	9.1	30.5	201	217	0.9	0.25-0.75	0.8-3.0

Acknowledgments

This research was supported by the National Center for Transportation Systems Productivity and Management (NCTSPM). NCTSPM is a collaboration between Georgia Institute of Technology, Georgia Transportation Institute, Florida International University, University of Central Florida, University of Alabama at Birmingham, and each university's state Department of Transportation. The instrumentation used for the experiments were funded by the National Science Foundation (NSF) [NSF MRI Award CMMI-0923365]. The authors acknowledge Dr. Emil Simiu for his suggestions to improve the manuscript. The authors also would like to acknowledge Walter Conklin, James Erwin, and Roy Liu Marques at the Wall of Wind (WOW) for their unreserved input during testing. The findings reported in this article are those of the authors alone, and do not necessarily represent the views of sponsoring agencies.

References

- AASHTO (2013), *Standard Specification for Structural Supports for Highway Signs, Luminaires, and Traffic Signals*, Washington, D.C.
- AASHTO (2009), *Standard Specifications for Structural Support for Highway Signs, Luminaires, and Traffic Signals*, Washington, DC.
- ASCE (2010), *Minimum Design Loads for Buildings and Other Structures*, New York, NY.
- Bearman, P.W. and Trueman D.M. (1972), "An investigation of the flow around rectangular cylinders", *Aeronautical Quarterly*, 229-237.
- Blevins, R.D. (1977), *Flow Induced Vibration*, New York: Van Nostrand Reinhold Company.
- Cao, S., Qiang, Z. and Zhiyong Z. (2014), "Velocity shear flow over rectangular cylinders with different side ratios", *Comput. Fluid.*, **96**, 35-46.
- Carassale, L., Freda, A. and Marrè-Brunenghi, M. (2013), "Effects of free-stream turbulence and corner shape on the galloping instability of square cylinders", *J. Wind Eng. Ind. Aerod.*, **123**, 274-280.
- Dexter, R.J. and Ricker, M.J. (2002), *NCHRP Report 469: Fatigue-Resistant Design of Cantilever Signal, Sign, and Light Supports*. University of Minnesota, Washington, D.C.: Transportation Research Board.
- Dyrbye, C. and Hansen, S.O. (1997), *Wind Loads on Structures*, Chichester, John Wiley & Sons, Ltd.
- Farquharson, F.B., Smith, F.C. and Vincent, G.S. (1950-1954), *Aerodynamic stability of suspension bridges with special reference to the Tacoma Narrows Bridge*, University of Washington Engineering Experiment Station, Bulletin No. 116, Parts I-IV.
- Fouad, F.H. and Calvert, E.A. (2001), *Evaluating the Design Safety of Highway Structural Supports*, Technical Report, Department of Civil & Engineering, University of Alabama at Birmingham, Tuscaloosa, AL: University Transportation Center for Alabama.
- Fouad, F.H. and Hosch, I.E. (2011), *Design of Overhead VMS Structures for Fatigue Loads*, Final report, Tuscaloosa: University Transportation Center for Alabama.
- Fouad, F.H., Davidson, J.S., Delatte, N., Calvert, E.A., Chen, S.E., Nunez, E. and Abdalla, R. (2003), *NCHRP Report 494: Structural Supports for Highway Signs, Luminaires, and Traffic Signals*, Technical

- Report, University of Alabama at Birmingham, Washington, D.C.: Transportation Research Board, 59.
- Fu, T. (2013), *Development of effective approaches to the large-scale aerodynamic testing of low-rise buildings*, PhD Thesis, Civil Engineering, Florida International University.
- Fu, T., Aly, A.M., Chowdhury, A.G., Bitsuamlak, G., Yeo, D. and Simiu, E. (2012), "A proposed technique for determining aerodynamic pressures on residential homes", *Wind Struct.*, **15**(1), 27-41.
- Gerrard, J.H. (1966), "The mechanics of the formation region of vortices behind bluff bodies", *J. Fluid Mech.*, **25**, 401-413.
- Ginal, S. (2003), *Fatigue Performance of Full-Span Sign Support Structures Considering Truck-Induced Gust and Natural Wind Pressures*, Ph.D. Thesis, Milwaukee: Marquette University.
- Irwin, P.A. (1998), "The role of wind tunnel modelling in the prediction of wind effects on bridges", *Proceedings of the International Symposium Advances in Bridge Aerodynamics*, Copenhagen, Balkema, Rotterdam.
- Kaczinski, M.R. and Dexter, R.J., Van Dien, J.P. (1998), *NCHRP Report 412: Fatigue-Resistant Design of Cantilevered Signal, Sign and Light Supports*, Technical Report, Lehigh University, Washington, D.C.: Transportation Research Board.
- Laneville, A., Gartshore, S. and Parkinson, G.V. (1975), "An explanation of some effects of turbulence on bluff bodies", *Wind Effects on Buildings and Structures*. London: Syndics of the Cambridge University Press. 333-341.
- Larose, G.L. and D'Auteuil, A. (2008), "Experiments on 2D rectangular prisms at high reynolds numbers in a pressurized wind tunnel", *J. Wind Eng. Ind. Aerod.*, **96**(6-7) 923-933.
- Liu, Z. and Kopp, G.A. (2010), "High-resolution vortex particle simulations of flows around rectangular cylinders", *Comput. Fluid.*, **40**(1), 2-11.
- Mannini, C., Marra, A.M. and Bartoli, G. (2014), "VIV - galloping instability of rectangular cylinders: Review and new experiments", *J. Wind Eng. Ind. Aerod.*, **132**, 109-124.
- Novak, M. (1972), "Galloping oscillations of prismatic structures", *J. Eng. Mech. Div. - ASCE*, **98**, 27-46.
- Parkinson, G.V. (1963), "Aeroelastic galloping in one dimension of freedom", *Proceedings of the International Conference on Wind Effects on Buildings and Structures*. Teddington, UK.
- Parkinson, G. (1989), "Phenomena and modelling of flow-induced vibrations of bluff bodies", *Prog. Aerospace Sci.*, **26**(2), 169-244.
- Smith, Douglas A., Delong Zuo, and Kishor C. Mehta. (2014), "Characteristics of net force and torques on a rectangular sign measured in the field", *J. Wind Eng. Ind. Aerod.*, **133**, 80-91.
- Taylor, Z.J., Gurka, R. and Kopp, G.A. (2014), "Effects of leading edge geometry on the vortex shedding frequency of an elongated bluff body at high Reynolds numbers", *J. Wind Eng. Ind. Aerod.*, **128**, 66-75.
- Yeo, D. and Chowdhury, A.G. (2013), "Simplified wind flow model for the estimation of aerodynamic effects on small structures", *J. Eng. Mech. -ASCE*, **139**(3), 367-375.
- Zuo, D. and Letchford, C. (2008), *Investigation of Wind-Induced Highway Lighting Pole Vibration Using Full-Scale Measurement*, Technical Report No. FHWA/TX-08-0-4586-5, College of Engineering, Texas Tech University, Austin, Texas: Texas Department of Transportation.
- Zuo, D., Smith, D.A. and Mehta, K.C. (2014), "Experimental study of wind loading of rectangular sign structures", *J. Wind Eng. Ind. Aerod.*, **130**, 62-74.